REFERENCES AND NOTES

1. J. J. Gibson, *Perception of the Visual World* (Houghton Mifflin, Boston, 1950).
2. W. H. Warren and D. J. Hannon, *Nature* **336**, 162 (1988).
3. C. S. Royden, M. S. Banks, J. A. Crowell, *ibid.* **360**, 583 (1992).
4. The eye-movement signal could be a copy of the smooth-pursuit command sent to the heading computation site, or a proprioceptive signal from the eye muscles and the periorbital tissue.
5. H. Saito *et al.*, *J. Neurosci.* **6**, 145 (1986).
6. M. S. Graziano, R. A. Andersen, R. J. Snowden, *ibid.* **14**, 54 (1994).
7. H. Sakata, H. Shibutani, K. Kawano, *J. Neurophysiol.* **49**, 1364 (1983).
8. H. Komatsu and R. H. Wurtz, *ibid.* **60**, 580 (1988).
9. W. T. Newsome, R. H. Wurtz, H. Komatsu, *ibid.*, p. 604.
10. C. J. Duffy and R. H. Wurtz, *J. Neurosci.* **15**, 5192 (1995).
11. The monkey was seated in a chair with its head fixed, facing a 100° by 100° projection screen. After maintaining fixation within a 5° by 5° window for the required time (3 s), the monkey was rewarded with a drop of water. Eye position was monitored with a scleral search coil [S. J. Judge *et al.*, *Vision Res.* **20**, 535 (1980)]. All procedures with animals were approved by the Caltech Institutional Animal Care and Use Committee.
12. Expanding random dot fields were generated by simulating the approach to a wall at 38 cm/s at a distance of 57 cm. This condition generated a radial speed of 15.7° per second at an eccentricity of 30° from the focus. Dot lifetimes were 300 ms (to limit acceleration cues), after which they were renewed at random locations. The stimulus was 50° by 50° square and contained 77 dots. The focus position was varied in 10° steps from −40° to 40° along an axis parallel to the neuron's preferred pursuit direction (distances are relative to the center of the stimulus, which was approximately centered in the neuron's spatial receptive field). For the ±30° and ±40° focus positions, the focus was situated outside the visible stimulus. We generated the stimulus for the simulated eye movements by moving the entire stimulus on the screen (by computer computation of the dot positions); this is equivalent to adding a constant-velocity component to each point in the flow field, which shifts the focus and causes the stimulus borders to move across the screen. The room was completely dark except for the stimulus.
13. Before studying a neuron's focus tuning, we determined its preferred pursuit direction by having the monkey follow a point moving at 0°, 45°, 90°, and so on, up to 315°. The direction eliciting the strongest response was taken as the preferred direction; the opposite direction was designated antipreferred.
14. Single neurons were monitored extracellularly with varnish-coated tungsten microelectrodes advanced dorsoventrally through the dura and into area MSTd, which was identified on the basis of receptive field size (most were >50° wide and crossed over the vertical meridian), flow preference (for example, expansion and rotation), position invariance, and modulation during smooth pursuit. Spike times were stored on a personal computer for subsequent analysis. All data are expressed as the mean firing rate during the middle 500 ms of a 1-s stimulus-presentation period. Results are based on a sample of 139 neurons from one hemisphere. These results are corroborated by recent data from a second animal (n = 18; K. S. Shenoy, D. C. Bradley, R. A. Andersen, *Soc. Neurosci. Abstr.*, in press).
15. In practice, all stimuli were presented in pseudorandom order.
16. "Screen coordinates" is an operational term. Because the monkey's eyes and head were in a constant position (except for the small eye displacement during pursuit), we cannot tell whether MSTd cells code for heading in eye, head, body, or world coordinates. Our results imply simply that these neurons account for eye movement, the first step necessary for computing the heading.
17. If we arbitrarily define retinal cells as shifting by −20°, −10°, or 0°, intermediate cells by 10° or 20°, and heading cells by 30°, 40°, or 50°, the percentages of the different cell types are about 42%, 31%, and 27%, respectively, where the shift estimate was based on maximum cross-correlation between the fixed- and moving-eye curves.
18. H. C. Longuet-Higgins and K. Prazdny, *Proc. R. Soc. London Ser. B* **208**, 385 (1980).
19. W. H. Warren, in *Perception of Space and Motion* (Academic Press, New York, 1995), chap. 3, pp. 263–325.
20. Because we did not correct for tangent error on the screen, dot speeds (for the pursuit target as well as the stimulus dots) were slightly underestimated at eccentric positions. However, this error was only ~8% at 12.5° eccentricity, ~20% in the corner (35° eccentricity), and 0 in the center. Therefore, the real and simulated pursuit conditions differed slightly in terms of the distribution of speeds across the retina.
21. To compute R_c for a given relative shift between curves, we correlated the responses on one curve with the responses on the other curve, pairing by x-axis value. Only overlapping regions of the curves could be cross-correlated. MSD was computed between corresponding data points on the two curves, again, only for overlapping regions.
22. A. Mack and E. Herman, *Vision Res.* **18**, 55 (1978).
23. T. C. A. Freeman, J. A. Crowell, M. S. Banks, *Invest. Ophthalmol. Vis. Sci.* **37**, S454 (1996).
24. Heading cell receptive fields also showed gain changes. In fitting our model (Fig. 4) to the heading cell data, these gain changes were taken into account, along with the receptive field shifts. It is uncertain whether these gain changes encode information about the heading; it is possible that they simply average to zero.
25. Sine functions were used because different parts of a sine function can approximate either a gaussian or a sigmoid function. Each sine function was characterized by amplitude, frequency, and phase, as well as by two "gain" parameters that were applied in the pursuit condition (one gain for each pursuit direction). All parameters were adjusted simultaneously, fitting three receptive fields (fixed-eye and two pursuit directions) concurrently, with the use of nonlinear least-squares regression. Analysis was done on a subset of 36 neurons, the receptive fields of which shifted during eye movements.
26. The speed of rotating patterns was scaled so that dot speed was identical to the expanding patterns (15.7°/s) at 30° eccentricity. Eye movements cause the focus in a rotating pattern to shift orthogonally to the eye movement. Therefore, for rotating patterns the focus was also varied orthogonally—otherwise it would not be possible to measure relative shifts between fixed- and moving-eye receptive fields.
27. Shifts were calculated on the basis of MSD.
28. Because the retinal focus shift depends on the pursuit speed and the rate of image expansion, receptive field shifts of different sizes are required to compute heading under different conditions. Because we tested only one pursuit and one expansion rate, we do not know whether individual receptive fields shift by varying amounts or whether a population code is used to read out the heading from different neurons depending on the pursuit and expansion rates.
29. Preliminary psychophysical experiments in our lab suggest that humans compensate at least partly for eye movements while pursuing across rotating stimuli.

30. We are grateful to D. Ward and B. Gillikin for technical assistance and to W. Warren and J. Crowell for helpful comments. This work was funded by the National Eye Institute, the Sloan Foundation for Theoretical Neurobiology at Caltech, the Office of Naval Research, and the Air Force Office of Scientific Research.

19 April 1996; accepted 19 July 1996

α Helix–RNA Major Groove Recognition in an HIV-1 Rev Peptide–RRE RNA Complex

John L. Battiste, Hongyuan Mao, N. Sambasiva Rao, Ruoying Tan, D. R. Muhandiram, Lewis E. Kay, Alan D. Frankel, James R. Williamson*

The solution structure of a human immunodeficiency virus type–1 (HIV-1) Rev peptide bound to stem-loop IIB of the Rev response element (RRE) RNA was solved by nuclear magnetic resonance spectroscopy. The Rev peptide has an α-helical conformation and binds in the major groove of the RNA near a purine-rich internal loop. Several arginine side chains make base-specific contacts, and an asparagine residue contacts a G·A base pair. The phosphate backbone adjacent to a G·G base pair adopts an unusual structure that allows the peptide to access a widened major groove. The structure formed by the two purine-purine base pairs of the RRE creates a distinctive binding pocket that the peptide can use for specific recognition.

RNA-protein interactions are central features of many fundamental biological processes, including translation, mRNA processing, and transcription. The HIV-1 Rev protein is an RNA-binding protein that regulates viral gene expression by affecting the relative amounts of spliced and unspliced mRNAs that are exported to the cytoplasm. Rev mediates its function by binding to the RRE RNA located within the *env* gene of HIV (*1*). Biochemical analyses have identified a high-affinity Rev-binding site in stem-loop IIB of the RRE (Fig. 1A) (*2*). Short α-helical peptides corresponding to the arginine-rich RNA-binding domain of Rev (Fig. 1B) bind specifically to this small RNA element (*3*), providing a good model system for structural analysis of the interaction by nuclear magnetic resonance (NMR) spectroscopy. A

structural understanding of the detailed interactions in this complex may assist in the design of therapeutics that inhibit this essential HIV-1 interaction.

For NMR analysis of the Rev peptide–RRE complex, the peptide was uniformly labeled with ^{13}C and ^{15}N by expression as a fusion protein in *Escherichia coli* (*4*, *5*) and assigned by means of triple-resonance NMR experiments (*6*). For complete assignment of the crowded arginine side chain resonances, an experiment was required to correlate all of the side chain carbons and protons to the ε-proton resonances, which are well resolved in the Rev-RRE complex (Fig. 2, A to C). Assignment and modeling of the bound RNA conformation using an unlabeled synthetic peptide have been described (*7*). To further refine the RNA structure, we obtained additional nuclear Overhauser effects (NOEs) from NMR experiments with ^{13}C- and ^{15}N-labeled RNA (*8*). Isotopically filtered NOE spectroscopy experiments were acquired on complexes with ^{13}C,^{15}N-labeled peptide (*6*) or ^{13}C-labeled RNA (*8*) to identify intermolecular NOEs. Three-dimensional models of the Rev-RRE complex were generated by using a hybrid distance geometry–stimulated annealing approach (*9*) with NMR-derived distance and dihedral restraints (*10*). Nineteen low-energy structures were obtained (Table 1), and a superposition of the coordinates (Fig. 2D) shows that the entire RNA-peptide complex is well ordered.

The Rev peptide binds the major groove of the RNA in an α-helical conformation, as indicated by previous circular dichroism studies (*3*, *11*). DNA-binding proteins often use α helices to recognize specific bases in the major groove (*12*). However, the major groove of an A-form RNA helix is deep and too narrow to accommodate an α helix, thus requiring non–Watson-Crick interactions to widen the groove (*13*). In the Rev-RRE complex, two purine-purine base pairs locally open the major groove, a process which appears to be facilitated by a pronounced distortion of the RNA backbone that results primarily from formation of the G48·G71 base pair in a locally parallel-stranded orientation (*7*). This distortion results in an S-shaped architecture to the backbone from nucleotides G70 to A73, an undertwisting of the base pairs in the internal loop, and an opening of the major groove by ~5 Å (Fig. 3) (*14*). The G·G base pair is important for Rev binding (*15*, *16*), yet it is not in direct contact with the peptide through hydrogen bonds, suggesting that it provides a critical structural feature for specific binding.

The Rev α helix penetrates much more deeply into the major groove than is typical of DNA-binding proteins. In contrast to the shallow major groove of a B-form DNA helix, the RRE internal loop retains the characteristic deep groove of A-form RNA, and the Rev peptide must bind deep within the groove to allow side chains to reach the bases. A comparison of the positioning of Rev and GCN4 α helices in the major groove (Fig. 3) reveals that the Rev helix is situated ~3 Å deeper than the GCN4 helix, which is representative of most DNA-binding recognition helices. In addition to binding deep within the groove, the Rev peptide

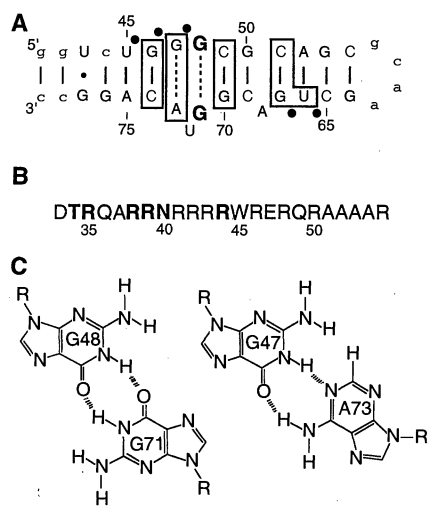

Fig. 1. Minimal RRE-Rev complex. (**A**) Sequence of RNA derived from stem-loop IIB of wild-type RRE (*29*). Boxed nucleotides were invariant in RNA selection studies of the Rev-RRE interaction in vitro, and the bold letters indicate a G·G base pair that was found to covary to an A·A base pair (*15*). Filled circles represent phosphates that interfere with Rev protein binding when ethylated (*17*). The numbering in the internal loop region is the same as for wild-type RRE, and non–wild-type nucleotides, in lowercase, are not numbered sequentially. (**B**) Sequence of the Rev peptide, which contains amino acids 34 through 50 of the RNA-binding domain. Bold letters indicate amino acids that result in a >10-fold decrease in binding specificity upon mutation to alanine (*3*). (**C**) Hydrogen-bonding arrangement of two purine-purine base pairs in the internal loop of the RRE determined from previous NMR analyses (*27*, *29*).

Table 1. Structural statistics and atomic root-mean-square (rms) deviations. Coordinates and modeling restraints have been deposited in the Protein Data Bank (ID code, 1ETF). <SA> are the 19 simulated-annealing structures, SA is the average structure before energy minimization, $(SA)_r$ is the restrained energy minimized average structure, and SD is standard deviation.

Parameter	<SA> ± SD	$(SA)_r$
Structural statistics		
Rms deviation from distance restraints (Å)*		
All (878)	0.015 ± 0.003	0.012
RNA (480)†	0.016 ± 0.002	0.012
Peptide (337)‡	0.011 ± 0.005	0.012
RNA-peptide (61)	0.017 ± 0.007	0.016
Rms deviation from dihedral restraints (degrees)		
All (111)§	0.57 ± 0.10	0.44
Rms deviation from idealized geometry		
Bonds (Å)	0.0034 ± 0.0001	0.0033
Angles (degrees)	0.031 ± 0.001	0.037
Impropers (degrees)	1.0 ± 0.2	0.65
Restraint violations‖		
Number of distance violations >0.1 Å	3.7 ± 2.3	2
Number of dihedral violations >2°	1.8 ± 1.4	0
Atomic rms deviations		
Region selected	<SA> vs. SA ± SD	<SA> vs. $(SA)_r$ ± SD
All heavy atoms	1.39 ± 0.12 Å	1.56 ± 0.15Å
Core¶	1.05 ± 0.10 Å	1.21 ± 0.11 Å

*In parentheses are the number of restraints used in the calculations. NOEs were classified into four distance-bound ranges based on visual inspection of cross-peak intensity: strong (1.8 to 3.0 Å), medium (1.8 to 4.0 Å), weak (1.8 to 5.0 Å), and very weak (1.8 to 6.0 Å). †Includes 210 intraresidue NOE, 184 interresidue NOE, and 86 hydrogen bond restraints. For the 43 base pair hydrogen bonds, both the heavy atom acceptor–to–hydrogen distance (1.7 to 2.2 Å) and heavy atom acceptor–to–heavy atom donor distance (2.7 to 3.2 Å) were restrained. ‡Includes 158 intraresidue NOE, 145 interresidue NOE, and 34 hydrogen bond restraints. For the 17 backbone hydrogen bonds, both the NH–CO distance (1.5 to 2.8 Å) and N–CO distance (2.4 to 3.5 Å) were restrained. §Includes 94 RNA sugar pucker and glycosidic bond torsions and 17 peptide Φ torsions. ‖There were no restraint violations >0.3 Å or >5° in <SA>. ¶The "core" of the complex is defined as heavy atoms in RNA nucleotides 44 to 53, 65 to 76, and peptide backbone atoms in amino acids 33 to 50.

J. L. Battiste, H. Mao, J. R. Williamson, Department of Chemistry, Massachusetts Institute of Technology, Cambridge, MA 02139, USA.
N. S. Rao, D. R. Muhandiram, L. E. Kay, Protein Engineering Centers of Excellence and Departments of Medical Genetics, Biochemistry, and Chemistry, University of Toronto, Toronto, Ontario, Canada M5S 1A8.
R. Tan and A. D. Frankel, Department of Biochemistry and Biophysics, University of California, San Francisco, CA 94143, USA.
*To whom correspondence should be addressed.

has an extensive interface with the RNA, interacting over three to four turns of the α helix.

Four amino acids make important base-specific contacts in the major groove (Fig. 4). The residues Arg^{35} and Arg^{39} interact with nucleotides U66, G67, and G70 on one side of the groove, and Asn^{40} and Arg^{44} interact with nucleotides U45, G46, G47, and A73 on the opposite side of the groove. Almost all of these nucleotides were invariant in in vitro selection experiments (*15*) or showed chemical modification interference of Rev binding (*16–18*). These important nucleotides all have functional groups within reasonable hydrogen-bonding distance of these four amino acids; however, the precision of the side chain positions is insufficient to determine exact hydrogen bond arrangements for these contacts. Nevertheless, Asn^{40} is clearly coplanar with the purine-purine G47·A73 base pair and makes hydrogen bonds to groups in the major groove. All four of the amino acids that make potential base-specific contacts are critical for peptide-binding specificity (*3*), and mutation of any of these three arginines to lysine results in a significant loss of binding activity in vivo, suggesting the existence of hydrogen bonds rather than simple electrostatic contacts (*11*).

In addition to the base-specific interactions, Thr^{34} and several arginines contact the phosphate backbone. In the average structure, the γ-OH of Thr^{34} is a potential hydrogen bond donor to a phosphodiester oxygen of G47 (Fig. 4A). Mutation of Thr^{34} results in a >10-fold decrease in binding specificity, and chemical modification of the G47 phosphate reduces binding specificity (*3*, *17*, *18*). Interestingly, Thr^{34} is also forming an "N-cap" structure at its NH_2-terminus that presumably stabilizes the α helix (*19*). NOEs and carbon chemical shifts typical of an N-cap (*20*) were observed for Thr^{34}, and in the average structure, the Oγ of Thr^{34} is a potential hydrogen bond acceptor for the backbone NH of Ala^{37} (Fig. 4A). The residue Thr^{34} is unique in the Rev peptide in that its side chain appears to make both peptide-peptide and RNA-peptide interactions.

In addition to Thr, there are six arginines (Arg^{38}, Arg^{41}, Arg^{42}, Arg^{43}, Arg^{46}, and Arg^{48}) that are positioned to make either hydrogen-bonding or simple electrostatic interactions with the phosphate backbone (Fig. 4B). Arginine-38 is positioned near the phosphates of U66 and G67, which both give chemical modification interference (*17*, *18*), and it is likely that Arg^{38} makes bridging hydrogen bonds between the two η-ni-

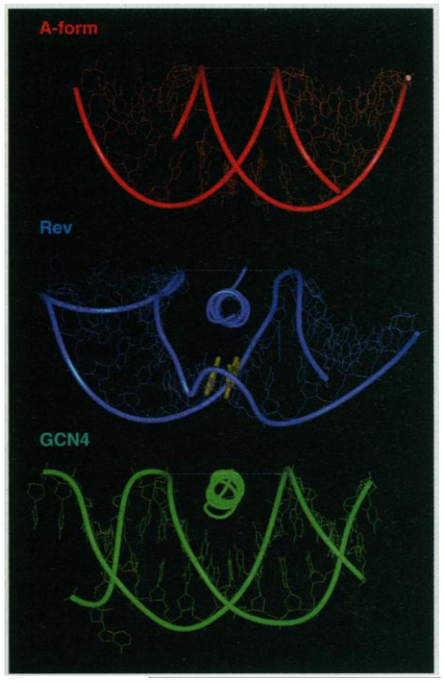

Fig. 3. RNA major groove width and depth. Views down the α helix axis of Rev (blue) and GCN4 (green) (*30*) with the major grooves of the RNA (or DNA) aligned with a standard A-form RNA duplex (red). The G48·G71 base pair is highlighted in yellow.

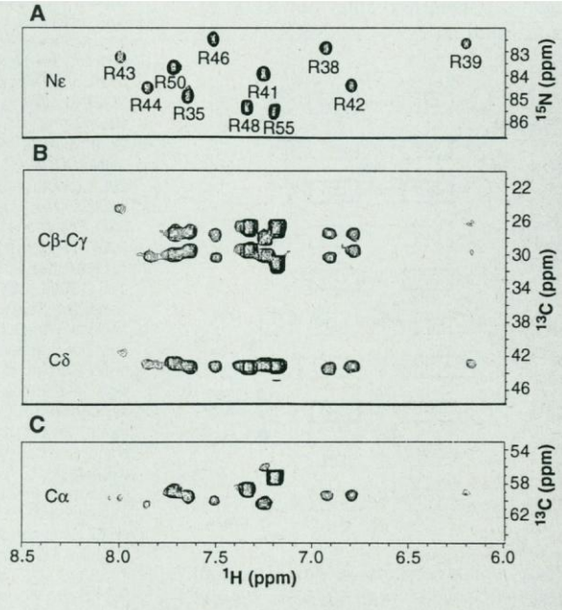

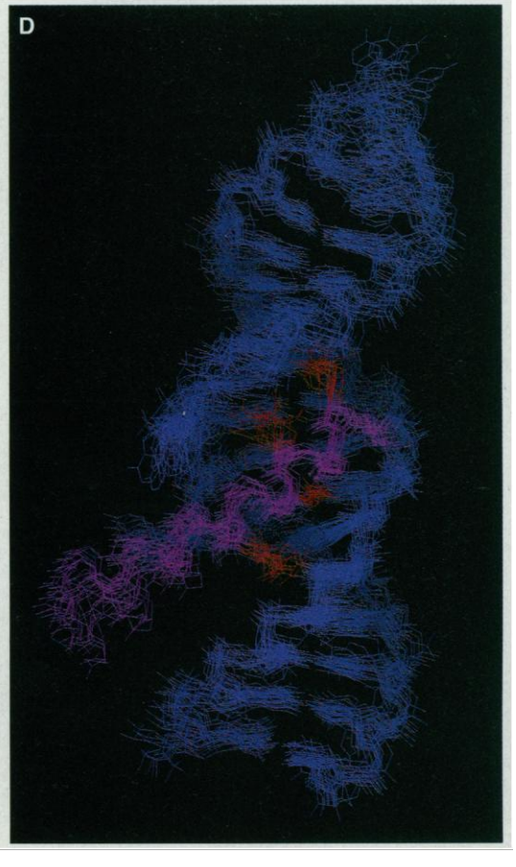

Fig. 2. NMR spectra for arginine assignment and superposition of simulated annealing structures. (**A**) Two-dimensional ^{15}N-heteronuclear single-quantum coherence (HSQC) spectrum of $^{13}C,^{15}N$-labeled Rev peptide–RRE RNA complex showing the well-resolved Nε-Hε correlations of the 11 arginine side chains. (**B**) Two-dimensional Arg-C(CC)-TOCSY-Nε-Hε spectrum with a short TOCSY mixing time and (**C**) with a long TOCSY mixing time correlating the β-, γ-, δ-carbons and α-carbon, respectively, to the ε-proton resonance of the arginine side chain. (**D**) Superposition of the 19 calculated structures on the average structure. All heavy atoms of the RNA (blue), backbone atoms of the peptide (magenta), and side chain heavy atoms of four amino acids making base-specific contacts (red) are shown. The view shows the major groove face of the internal loop of the RNA with the NH_2-terminus of the peptide at the upper right.

trogens and the phosphodiester oxygens of U66 and G67, because it cannot be functionally substituted by lysine (*11*). Arginine-38 and Thr^{34} make phosphate contacts flanking the region of the base-specific contacts and probably stabilize this region of the peptide. An especially arginine-rich face of the α helix makes phosphate contacts on the 3′ side of the hairpin containing two single-nucleotide bulges, which brings many phosphates in close proximity (Fig. 4B). In particular, Arg^{46} probably stabilizes the unfavorable electrostatic interactions near the U72 bulge, where the phosphorus atoms of G70 and U72 are ~4 Å apart. Mutation of Arg^{46} to alanine, but not to lysine, results in a sevenfold decrease in binding specificity, consistent with a specific electrostatic contact (*11*). In addition, Arg^{46}, Arg^{48}, and Arg^{50} at the COOH-terminus of the peptide, which mutational data suggest are moderately important for specific binding (*3*), are making phosphate and van der Waals contacts that may help orient the isolated α helix in the groove.

The arginine-rich motif (ARM) is defined solely by a short region containing a high density of arginines. There are now two structural examples of short ARM peptides bound to RNA, bovine immunodeficiency virus Tat-TAR (trans-acting region) (*21*) and HIV-1 Rev-RRE, and each peptide adopts a different secondary structure (β hairpin and α helix, respectively). Therefore, the ARM does not represent a unique structural motif (*10*, *22*). Despite the differences, both peptides bind deeply in the major groove, and the high density of arginines characteristic of the ARM may be important for charge neutralization as the peptide penetrates the deep groove and forms a large interface. This feature probably also allows these 10– to 20–amino acid ARM peptides to bind as structurally independent elements, which is another characteristic feature of the ARM. The distinctive RNA structures formed by the binding sites undoubtedly also contribute to the folding and binding of these small ARM peptides.

Recognition of distinctive structural features of RNA has been observed in most studies of RNA-protein complexes. For example, tRNA synthetases recognize the L-shape of tRNA, and $tRNA^{Ser}$ is also recognized in part by its long variable arm extension (*23*). In HIV-1 TAR, a base triple is proposed to be an integral part of the binding site for arginine, but it does not hydrogen bond to the arginine (*24*). In the RRE, the G48·G71 base pair is structurally important to widen the major groove but does not directly contact the peptide. Overall, the structure surrounding the two purine-purine base pairs may provide a deep binding pocket and a distinctive shape to the major groove that the peptide can use for specific recognition. It is remarkable that RNA elements as small as TAR and RRE can provide such specific three-dimensional frameworks for protein binding, and the Rev-RRE complex once again highlights the importance of RNA structure for protein recognition.

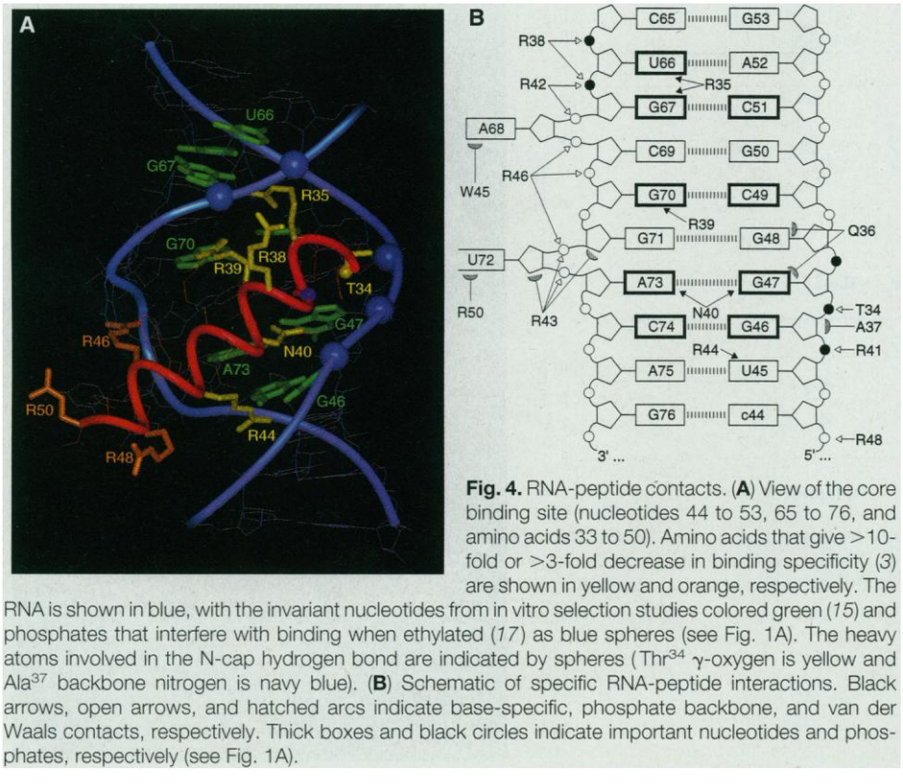

Fig. 4. RNA-peptide contacts. (**A**) View of the core binding site (nucleotides 44 to 53, 65 to 76, and amino acids 33 to 50). Amino acids that give >10-fold or >3-fold decrease in binding specificity (*3*) are shown in yellow and orange, respectively. The RNA is shown in blue, with the invariant nucleotides from in vitro selection studies colored green (*15*) and phosphates that interfere with binding when ethylated (*17*) as blue spheres (see Fig. 1A). The heavy atoms involved in the N-cap hydrogen bond are indicated by spheres (Thr^{34} γ-oxygen is yellow and Ala^{37} backbone nitrogen is navy blue). (**B**) Schematic of specific RNA-peptide interactions. Black arrows, open arrows, and hatched arcs indicate base-specific, phosphate backbone, and van der Waals contacts, respectively. Thick boxes and black circles indicate important nucleotides and phosphates, respectively (see Fig. 1A).

REFERENCES AND NOTES

1. H. S. Olsen, A. W. Cochrane, P. J. Dillon, C. M. Nalin, C. A. Rosen, *Genes Dev.* **4**, 1357 (1990); M. L. Zapp, T. J. Hope, T. G. Parslow, M. R. Green, *Proc. Natl. Acad. Sci. U.S.A.* **88**, 7734 (1991).
2. K. S. Cook *et al.*, *Nucleic Acids Res.* **19**, 1577 (1991); L. S. Tiley, M. H. Malim, H. K. Tewary, P. G. Stockley, B. R. Cullen, *Proc. Natl. Acad. Sci. U.S.A.* **89**, 758 (1992).
3. R. Tan, L. Chen, J. A. Buettner, D. Hudson, A. D. Frankel, *Cell* **73**, 1031 (1993).
4. Rev peptides were expressed as COOH-terminal fusions with a modified, His-tagged TrpLE leader polypeptide. Oligonucleotides encoding the Rev peptide (Fig. 1B) were inserted into the pMM vector for expression of unlabeled peptides (*25*) or the pTM vector for expression of isotopically labeled peptides (M. A. Milhollen and P. S. Kim, unpublished results). ^{15}N- or $^{13}C,^{15}N$-labeled peptides were expressed in M9 minimal media supplemented with either ^{13}C-glucose (1.0 g/liter) or ^{15}N-ammonium sulfate (0.7 g/liter), or both (Cambridge Isotope Laboratories). Peptides were isolated and purified as described (*25*). Yields of peptide per liter of culture were ~10 mg and ~4 mg for unlabeled and labeled peptide, respectively.
5. Previous biochemical analyses of the Rev-RRE complex were performed with synthetic peptides containing modified termini that increased α-helicity and RNA-binding specificity (*3*, *11*). The expressed peptide used here contains an aspartic acid at its NH_2-terminus to mimic the succinyl modification of the synthetic peptide. The α-helical content of the unbound expressed peptide is ~12% as measured by circular dichroism [10 mM $NaPO_4$ (pH 6.5), 100 mM NaF, 5°C] (*26*), compared with ~50% for the modified synthetic peptide (*3*). Despite the lower α-helical content, the expressed peptide retains specific RNA-binding activity and gives RNA chemical shifts and NOEs identical to a complex with the synthetic peptide (*7*).
6. Complexes of $^{13}C,^{15}N$-labeled Rev peptide with unlabeled RNA (1:1) were prepared as described (*6*, *29*), except that the pH was 5.5. Three-dimensional H(C)(CO)NH–TOCSY [G. T. Montelione, B. A. Lyons, S. D. Emerson, M. Tashiro, *J. Am. Chem. Soc.* **114**, 10974 (1992)], (H)C(CO)NH-TOCSY [T. M. Logan, E. T. Olejniczak, R. X. Xu, S. W. Fesik, *FEBS Lett.* **314**, 413 (1992)], CBCANH [M. Wittekind and L. Mueller, *J. Magn. Reson. B* **101**, 201 (1993); D. R. Muhandiram and L. E. Kay, *ibid.* **103**, 201 (1994)], and two-dimensional Arg-C(CC)-TOCSY-Nε-Hε through-bond correlation experiments were performed to assign all resonances of the peptide. Details of the assignment of the peptide and the arginine experiments will be published separately. A three-dimensional simultaneously $^{13}C,^{15}N$-edited NOESY-HSQC experiment (*28*) [mixing time (τ_M) = 150 ms) was performed to obtain NOEs for the peptide. A simultaneously $^{13}C,^{15}N$-F1–filtered,F3-edited-NOESY-HSQC was performed to identify RNA-peptide NOEs [(*28*); M. Ikura and A. Bax, *J. Am. Chem. Soc.* **114**, 2433 (1992)]. To obtain ϕ torsion restraints for the peptide backbone, a HNHA experiment [G. W. Vuister and A. Bax, *ibid.* **115**, 7772 (1993)] was performed on a ^{15}N-labeled Rev peptide sample. α→NH(i,i+3) and α→β(i,i+3) backbone NOEs, small HN-Hα coupling constants (~4 Hz), and deviations of α-carbon and α-proton chemical shifts from random coil [D. S. Wishart, B. D. Sykes, F. M. Richards, *Biochemistry* **31**, 1647 (1992); D. S. Wishart and B. D. Sykes, *J. Biomol. NMR* **4**, 171 (1994)] characteristic of a continuous α helix from Arg^{35} to Arg^{55} were observed.
7. J. L. Battiste, R. Tan, A. D. Frankel, J. R. Williamson, *J. Biomol. NMR* **6**, 375 (1995).

8. Experiments with ^{13}C- or ^{15}N-labeled RNA were performed on 500- or 600-MHz NMR instruments at the Francis Bitter National Magnet Laboratory or a Varian Unity-Plus 750-MHz instrument. A three-dimensional NOESY-HSQC [G. M. Clore, A. Bax, P. C. Driscoll, P. T. Wingfield, A. M. Gronenborn, *Biochemistry* **29**, 8172 (1990)] (τ_M = 200 ms), a four-dimensional HMQC-NOESY-HSQC [G. W. Vuister *et al.*, *J. Magn. Reson. B* **101**, 210 (1993)] (τ_M = 150 ms), and a two-dimensional double-half-filter NOESY experiment [G. Otting and K. Wuthrich, *Q. Rev. Biophys.* **23**, 39 (1990)] (τ_M = 200 ms) with ^{13}C-labeled RNA and expressed Rev peptide were performed to obtain NOEs for molecular modeling. A three-dimensional NOESY-HSQC [S. Mori, C. Abeygunawardana, M. O. Johnson, P. C. M. v. Zijl, *J. Magn. Reson. B* **108**, 94 (1995)] (τ_M = 150 ms) with ^{15}N-labeled RNA was also obtained.
9. M. Nilges, G. M. Clore, A. M. Gronenborn, *FEBS Lett.* **229**, 317 (1988).
10. Molecular modeling was performed with the DGII and DISCOVER modules of Insight II (Biosym). The force constants for NMR-derived distance and torsion restraints were 10 kcal mol^{-1} Å^{-2} and 60 kcal mol^{-1} degree^{-2}, respectively. No nonexperimental torsion restraints were used to enforce A-form geometry for any region of the RNA. A quartic repulsive function was used for nonbonding contacts in all calculations, and electrostatic interactions were completely neglected. A total of 140 distance geometry structures were generated and input into a high-temperature (1000 K) simulated-annealing protocol using the AMBER forcefield with the masses for all the atoms set to 100 [A. T. Brunger, *X-PLOR User Manual, Version 3.1* (Yale Univ. Press, New Haven, CT, 1992)]. The force constants for the covalent geometry, distance and dihedral, and nonbonded terms were sequentially scaled from 1% to full value over 36 ps of dynamics in 3-fs steps. The temperature was then cooled to 10 K over 21 ps. The 30 structures with the lowest NMR restraint violation energies were chosen for further refinement. Peptide hydrogen bonds were added for the well-defined α helix at this stage. The refinement protocol consisted of 6 ps of dynamics (1-fs steps) at 500 K, scaling the nonbonded terms from 10% to full value. The temperature was then exponentially cooled to 10 K over 9 ps, followed by 100 and 500 steps of steepest and conjugate gradient minimization, respectively. The 19 structures with the lowest restraint violation energies and no violations >0.3 Å were chosen for detailed structural analysis. An average structure (SA) was generated by superimposing the coordinates of all 19 structures and then averaging the coordinates. The covalent geometry of the average structure was regularized by 100 steps of steepest descent and 500 steps of conjugate gradient minimization.
11. R. Tan and A. Frankel, *Biochemistry* **33**, 14579 (1994).
12. C. O. Pabo and R. T. Sauer, *Annu. Rev. Biochem.* **61**, 1053 (1992).
13. K. M. Weeks and D. M. Crothers, *Science* **261**, 1574 (1993).
14. The major groove width of the RNA was quantitated by measuring the shortest phosphorus atom distances across the groove and subtracting 5.8 Å for the van der Waals radii of the phosphate group.
15. D. P. Bartel, M. L. Zapp, M. R. Green, J. W. Szostak, *Cell* **67**, 529 (1991).
16. S. Iwai, C. Pritchard, D. A. Mann, J. Karn, M. J. Gait, *Nucleic Acids Res.* **20**, 6465 (1992).
17. J. Kjems, B. J. Calnan, A. D. Frankel, P. A. Sharp, *EMBO J.* **11**, 1119 (1992).
18. C. E. Pritchard *et al.*, *Nucleic Acids Res.* **22**, 2592 (1994).
19. E. T. Harper and G. D. Rose, *Biochemistry* **32**, 7605 (1993).
20. P. C. Lyu and D. E. Wemmer, *ibid.*, p. 421; A. M. Gronenborn and G. M. Clore, *J. Biomol. NMR* **4**, 455 (1994).
21. J. D. Puglisi, L. Chen, S. Blanchard, A. D. Frankel, *Science* **270**, 1200 (1995); X. Ye, R. A. Kumar; D. J. Patel, *Chem. Biol.* **2**, 827 (1995).
22. L. Chen and A. D. Frankel, *Proc. Natl. Acad. Sci. U.S.A.* **92**, 5077 (1995); R. Tan and A. D. Frankel, *ibid.*, p. 5282; K. Harada, S. A. Martin, A. D. Frankel, *Nature* **380**, 175 (1996).
23. M. A. Rould, J. J. Perona, D. Söll, T. A. Steitz, *Science* **246**, 1135 (1989); M. Ruff *et al.*, *ibid.* **252**, 1682 (1991); V. Biou, A. Yaremchuk, M. Tukalo, S. Cusack, *ibid.* **263**, 1404 (1994).
24. J. D. Puglisi, R. Tan, B. J. Calnan, A. D. Frankel, J. R. Williamson, *ibid.* **257**, 76 (1992); J. D. Puglisi, L. Chen, A. D. Frankel, J. R. Williamson, *Proc. Natl. Acad. Sci. U.S.A.* **90**, 3680 (1993).
25. J. P. Staley and P. S. Kim, *Protein Sci.* **3**, 1822 (1994); T. N. M. Schumacher *et al.*, *Science* **271**, 1854 (1996).
26. J. L. Battiste, data not shown.
27. R. D. Peterson *et al.*, *Biochemistry* **33**, 5357 (1994).
28. S. M. Pascal, D. R. Muhandiram, T. Yamazuki, J. D. Forman-Kay, L. E. Kay, *J. Magn. Reson. B* **103**, 197 (1994).
29. J. L. Battiste, R. Tan, A. D. Frankel, J. R. Williamson, *Biochemistry* **33**, 2741 (1994).
30. T. E. Ellenberger *et al.*, *Cell* **71**, 1223 (1992).
31. We thank J. Puglisi for helpful discussions, C. Turner and A. Brodsky for assistance with NMR experiments, M. Milhollen and P. Kim for providing the pMM and pTM plasmids, M. Oakley and C. Cilley for assistance in purification of peptides, and C. Pabo for critical comments. J.L.B. was supported in part by the NIH Interdepartmental Biotechnology Program (GM-08344), and R.T. is a Scholar for the American Foundation for AIDS Research (70405-15-RF). Supported by grants from the National Sciences and Engineering Research Council of Canada (L.E.K.), the Medical Research Council of Canada (L.E.K.), the Searle Scholars Program of the Chicago Community Trust (J.R.W.), and NIH grants GM-39589 (A.D.F. and J.R.W.) and GM-53320 (J.R.W.).

26 June 1996; accepted 15 August 1996

Regulation of Integrin Function by the Urokinase Receptor

Ying Wei, Matvey Lukashev, Daniel I. Simon, Sarah C. Bodary, Steven Rosenberg, Michael V. Doyle, Harold A. Chapman*

Integrin function is central to inflammation, immunity, and tumor progression. The urokinase-type plasminogen activator receptor (uPAR) and integrins formed stable complexes that both inhibited native integrin adhesive function and promoted adhesion to vitronectin via a ligand binding site on uPAR. Interaction of soluble uPAR with the active conformer of integrins mimicked the inhibitory effects of membrane uPAR. Both uPAR-mediated adhesion and altered integrin function were blocked by a peptide that bound to uPAR and disrupted complexes. These data provide a paradigm for regulation of integrins in which a nonintegrin membrane receptor interacts with and modifies the function of activated integrins.

Receptors of the integrin family mediate adhesion of cells to extracellular matrices as well as intercellular interactions, and modulate transduction of regulatory signals that are central to inflammation, immunity, hemostasis, and tumor progression. In mediating these functions, integrin receptors undergo regulated and reversible activation as a result of ligand binding or cellular stimulation by chemoattractants (*1*). Activation is characterized by conformational changes in the integrin extracellular domains, reorganization of intracytoplasmic connections, and redistribution of integrins on the cell surface, which together augment integrin avidity for ligands (*2*). Dynamic activation of integrins is central to integrin-mediated adhesion and migration (*1*), although little is known about functionally important interactions of integrins with other membrane proteins that might regulate this process. We have now identified a pathway of interaction between activated integrins and a nonintegrin receptor that regulates integrin function.

The urokinase receptor (uPAR) is a glycosyl-phosphatidylinositol (GPI)–linked cell surface protein that is expressed in many cell types and is spatially and temporally associated with cellular structures that regulate cell adhesion, migration, and invasion (*3*). Previously, we have shown that uPAR can function as an adhesion receptor for vitronectin, with the vitronectin binding site being distinct from the urokinase binding site (*4*, *5*). uPAR colocalizes with integrins in focal contacts, at the leading edge of migrating cells, and in antibody-induced clusters (*6*). The receptor copurifies with and influences the function of the leukocyte integrin Mac-1, suggesting that it interacts functionally with this integrin (*7*). We hypothesized that formation of complexes between uPAR, which does not contain a transmembrane domain, and integrins might provide an integrin-mediated link between uPAR and the cytoskeleton

Y. Wei, D. I. Simon, H. A. Chapman, Department of Medicine, Brigham and Women's Hospital and Harvard Medical School, Boston, MA 02115, USA.
M. Lukashev, Department of Stomatology, University of California, San Francisco, CA 94143, USA.
S. C. Bodary, Genentech, South San Francisco, CA 94080, USA.
S. Rosenberg and M. V. Doyle, Chiron Corporation, Emeryville, CA 94608, USA.

*To whom correspondence should be addressed at Brigham and Women's Hospital, Room 703, Thorn Research Building, 20 Shattuck Street, Boston, MA 02115, USA.